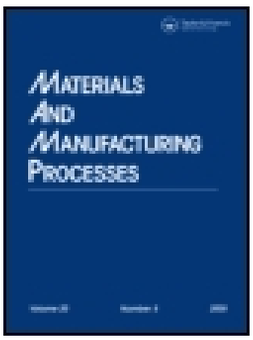

Materials and Manufacturing Processes

ISSN: (Print) (Online) Journal homepage: https://www.tandfonline.com/loi/lmmp20

Milling force model for asymmetric end-mills during high-feed milling on AISI-P20

Diego Russo, Gorka Urbicain, Antonio J. Sánchez Egea, Alejandro Simoncelli & Daniel Martinez Krahmer

To cite this article: Diego Russo, Gorka Urbicain, Antonio J. Sánchez Egea, Alejandro Simoncelli & Daniel Martinez Krahmer (2021): Milling force model for asymmetric end-mills during high-feed milling on AISI-P20, Materials and Manufacturing Processes, DOI: 10.1080/10426914.2021.1944199

To link to this article: https://doi.org/10.1080/10426914.2021.1944199

Published online: 29 Jun 2021.

MATERIALS AND MANUFACTURING PROCESSES
https://doi.org/10.1080/10426914.2021.1944199

Taylor & Francis
Taylor & Francis Group

Milling force model for asymmetric end-mills during high-feed milling on AISI-P20

Diego Russo[a], Gorka Urbicain[b], Antonio J. Sánchez Egea[c], Alejandro Simoncelli[d,e], and Daniel Martinez Krahmer[d,e]

[a]Faculty of Engineering, Universidad Nacional de la Matanza, San Justo, Argentina; [b]Department of Mechanical Engineering, Faculty of Engineering of Bilbao, Aeronautics Advanced Manufacturing Center (CFAA), Bilbao, Spain; [c]Department of Mechanical Engineering (EEBE), Universitat Politècnica de Catalunya, Barcelona, Spain; [d]Center for Research and Development in Mechanics, National Institute of Industrial Technology (INTI), Buenos Aires, Argentina; [e]Faculty of Engineering, Universidad Nacional de Lomas de Zamora, Buenos Aires, Argentina

ABSTRACT

Manufacturing molds for plastic parts injection are a particular machining domain, where challenging materials, like AISI P20 steel, are forced to satisfy the highest surface quality requirements. Before mirror polishing, milling operation is a common and challenging task due to drilling and milling with the same tool. Thus, special cutting tools, like asymmetric indexable type, are often used. This tool presents two geometrically equal positive inserts – one placed horizontally and the other vertically – for the flexible machining of holes, cavities, floors, and walls. Rough-medium milling operations lead to a complicated relationship between cutting conditions and geometrical tool parameters, making it challenging to balance the tool life of both inserts. The novelty of this work is to propose a model for cutting force prediction with an asymmetric tool to explain the separated behavior of both inserts and determine a better compromise between cutting conditions and tool life. The experimental tests were done for model validation and then wear cutting tests for testing improved cutting conditions. The results predicted by the model proved that by changing the depth of cut from 0.3 mm to 0.8 mm, the wear in both inserts was more balanced, increasing chip volume up to 1.7 times.

ARTICLE HISTORY
Received 7 April 2021
Accepted 1 June 2021

KEYWORDS
Asymmetric; end-mill; AISI-P20; forces; wear; modeling

Introduction

The production of plastic parts is growing steadily for many years.[1] The real dimension of this remarkable increase is compared with the materials used to manufacture parts of a car produced in the 90s with respect to the parts manufactured today, which fulfil similar functions. Many metal parts have been replaced by polymers, as is the case with bumpers. On top of that, methods of mass production of these pieces have been added in recent years, which are obtained by injection in very complex molds manufactured in tool steels.[2] Among the steels used for manufacturing dies for plastic parts injection, AISI P20 steel is the most widely used.[3] This kind of steel stands out mainly for its capability of being polished, where mirror polishing of the surface roughness is crucial for these dies. Also, highlight that the polishability improves significantly when the steel has a low content of inclusions (microstructural cleanliness), its microstructure and chemical segregation are homogeneous, and it is possible to obtain a high surface hardness, preferably above 40 HRC,[4] after the respective heat treatment.

Machining and polishing represent 80% of the total cost of plastic injection matrix production.[4] Injection dies for plastic parts made of AISI P20 steel are made by EDM[5] and mainly machined by milling. These dies require machining to transform the starting material into a finished mold.[6] To reduce this percentage of cost, steel mills have developed two variants of AISI P20 steel, one designated as AISI P20 + S steel to improve machinability and the other designated as AISI P20+ Ni steel to increase its polishability.[7] For the first case, sulfur addition reduces wear on the edge of the tool tip.[8] Regarding free-cutting steels, where MnS in the microstructure is adhered to the leading face of the cutting tool, forming a tribofilm and acting as a solid self-lubricant.[9,10] Instead, the polishability of AISI P20 + S steel is significantly impaired. As for the second case, AISI P20+ Ni steel allows generating a substantial improvement of the polishability.[4] Consequently, manufacturers choose between the variant of AISI P20 steel with sulfur or with nickel depending on the type of piece to manufacture, the desired surface finishing and the number of pieces to produce. An increase in machinability leads to a decrease in polishability and the other way around. There are also other alternatives to continue improving the properties of this material. Thus, Priyadarshini et al.[11] applied a cryogenic treatment to an AISI P20 steel and obtained a 28% improvement in the wear resistance measured in pin-on disk tests. Also, Park et al.[12] utilized a diode laser to modify the surface characteristics of an AISI P20 steel and the block-on-ring tests. They found a decrease in the friction coefficient from 0.5 to 0.33 compared with the untreated steel. In the same research topic, Yan et al.[13] used ball-on disk tests to study the influence of nitriding treatment on the surface modified by an ionic laser. They denoted 43% of wear when testing the surface without nitriding. High-feed milling is an option used in rough face milling to increase machining removal rate on flat surfaces with a large area, as for producing molds and dies, engine blocks, flanges, and

CONTACT Antonio J. Sánchez Egea antonio.egea@upc.edu Department of Mechanical Engineering (EEBE), Universitat Politècnica de Catalunya, Av. D'Eduard Maristany, 16, Barcelona 08019, Spain

machine guide-ways.[14] High-feed milling allows maintaining a high removal rate, employing a moderate cutting speed which produces a prolonged tool edge life.[15] Cut these dies is challenging due to the complex geometry, where at the beginning come from prismatic hardened and tempered blanks with an average hardness of 30 HRC and could be machined with coated hard metal inserts with ISO P quality.[16] Drilling these dies is also an essential operation since it allows to generate the holes that serve as guides of the die.[17] Arruda and coworkers[18] studied the process conditions that allow the best degree of surface roughness to achieve using carbide spherical milling cutters, typical in finishing milling of cavities. The proper selection of the cutting parameters in high feed milling is crucial for reducing machining time to reduce tool costs.[19] For instance, Abou-El-Hossein[20] investigated the cutting force in the end-milling operation of modified AISI P20 steel. They proposed a model to predict these cutting forces based on four inputs the cutting speed, feed rate, radial depth, and axial depth of cut; although no similar works on predict cutting forces have been found for asymmetric tools in milling operations.

Despite that milling operation with asymmetric tools has not taken much attention in the literature, these tools present great versatility due to using high feed rates and increasing machining efficiency. For example, Zou et al.[21] investigated the milling an AISI D2 steel with an asymmetric carbide insert mill coated with TiNAl. They used comparable cutting conditions (condition 3) and observed a wear difference on the flank between the smaller and larger insert of the order of 95% after removing 186 cm^3 of chip. Recently, Plodzien et al.[22] studied the material removal rate, cutting forces and surface properties when using a conventional and an asymmetric milling cutter. They noted that an asymmetric cutter presented higher cutting forces and increased by twice the chip flow rate. Conversely, it was also denoted higher surface roughness due to higher vibration amplitudes that can alter the service life of this asymmetric tool. Nevertheless, the way these tools behave during cutting becomes complex to understand, leading to different wear mechanisms that take into account not only vibration. In light of all of this, the core objective of this work is to propose an asymmetric milling force model to predict cutting forces in high feed milling of hard-to-cut material, like AISI P20. Thus, the proposed force model allows choosing the cutting conditions that improve the balance of tool degradation between the two oriented PVD-coated carbide inserts and extend their life service.

Materials and methods

This research motivation arises during the machining of AISI P20 + Ni steel molds intended for injecting plastic parts. Machining these molds is carried out on materials whose hardness is around 30 HRC hardness. The semi-roughing milling process is done using a flexible asymmetric milling cutter having two inserts placed in horizontal (H-insert) and vertical (V–insert) directions (see Fig. 1). This type of tool is selected due to its flexibility in terms of machining operations. Indeed, it is capable of performing boring, face milling or squaring operations, among others.

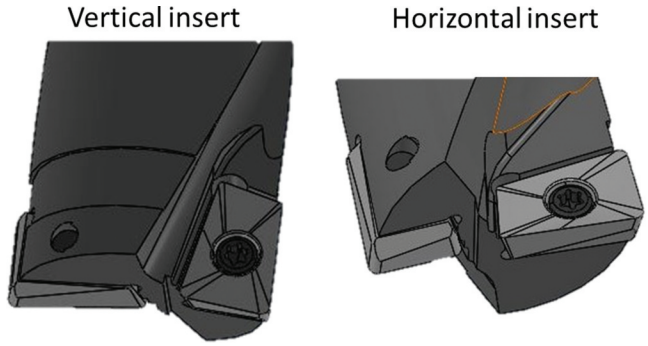

Figure 1. Asymmetric cutting tool with two inserts: both inserts are similar but with a vertical and horizontal orientation.

After machining many molds with the following machining conditions: a_p = .3 mm; a_e = 18 mm; V_c = 700 mm/min; spindle speed of 1300 rpm and dry cutting condition, uneven wear occurs on the cutting edges of the inserts. The insert in the horizontal direction presented extensive wear of the tool tip compared to the insert oriented in the vertical direction. Figure 2 shows the difference in wear progression in the cutting edge of both inserts when used 0.3 mm of cutting depth (initial condition) for approximately 95 minutes. After that time, the H-insert presented significant wear in its cutting edge. Instead, the vertical insert did not reach the maximum flank wear criterium (V_{Bmax}) to replace the insert. The wear progression in the V–insert is less pronounced, one V–insert every three H-inserts leading to accelerated costs due to H-insert replacing.

The asymmetric tools with AlTiN coated inserts (type QOMT 1342 R-M2 and quality MP 6120 equivalent to ISO P20) and specific tool-holder (type AQXR25) were used during the experiments. The weight, volume, and density of the insert were 3.4 ± 0.1 g, 0.2471 cm^3 and 13.76 g/cm^3, respectively. The substrate has a hardness of 91.5 HRA and a transverse rupture strength toughness of 2.5 GPa. The milling tests were performed under the following conditions: milling cutter of 25 mm diameter with two coated carbide inserts, a spindle speed of 1300 rpm (V_c = 102 m/min), a feed rate of 700 mm/min (feed per tooth 0.27 mm/v) and a milling width of 18 mm. Table 1 lists the main geometrical parameter of the used asymmetric cutting tool. Table 2 shows the chemical composition of the substrate and coating used for the insert. Table 3 shows the chemical composition of the material to be cut (AISI P20 + Ni).[23]

Results and discussion

Cutting forces are modeled using a mechanistic method,[24,25] where cutting coefficients need to be calibrated. These models raise differential force elements in tool rotating system *tra*, which then need to be 1) integrated for the cutting length engaged in the cut and 2) transformed to an inertial system *xyz*. Besides, the contribution of the different inserts engaged during the cut needs to be considered.

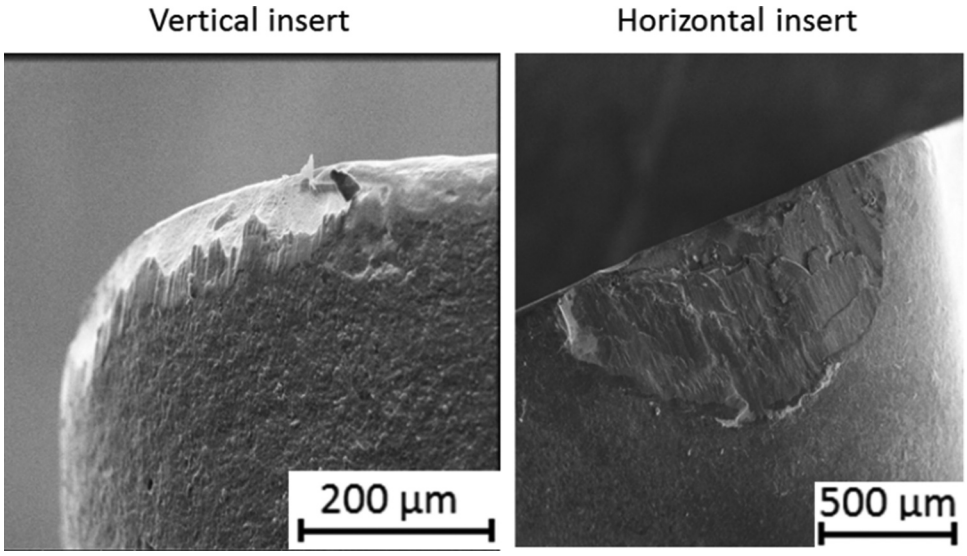

Figure 2. Wear at the cutting edge in the vertical and horizontal oriented inserts after 95 minutes of high feed milling with 0.3 mm of depth of cut.

Table 1. Geometric parameters of the asymmetric tool.

Insert	Diameter [mm]	Helix angle [°]	Corner radius [mm]	Starts at z [mm]	Rake angle [°]
H	25	17	0.8	0	0 (N)
V	25	18	0.8	0.15	negative

Table 3. Chemical composition of the material to cut (AISI P20 + Ni) .[21].

Material	%wt C	%wt Si	%wt Mn	%wt Cr	%wt Mo	%wt Ni
AISI P20 + Ni	0.38	0.30	1.50	2.00	0.20	1.10

The cutting forces acting on an infinitesimal edge element are divided into shear and friction elements in the three-tangential, radial, and axial–directions:

$$\begin{aligned} dF_{t,j}\left(\phi_j,\kappa\right) &= K_{tc}h\left(\phi_j,\kappa\right)db + K_{te}ds \\ dF_{r,j}\left(\phi_j,\kappa\right) &= K_{rc}h\left(\phi_j,\kappa\right)db + K_{re}ds \\ dF_{a,j}\left(\phi_j,\kappa\right) &= K_{ac}h\left(\phi_j,\kappa\right)db + K_{ae}ds \end{aligned} \tag{1}$$

For straight cutting inserts ($\kappa = 90°$), h is the theoretical and varying chip thickness computed as $h = f_z \cdot sin\phi_j$, while db is a discrete axial element ($db = dz$) necessary for the numerical integration. The accompanying term to friction contribution ds is the cutting-edge differential element.

The model raised here is built from the following assumptions:

(1) Asymmetric behavior means different cutting coefficients need to be calculated separately for the H- and V–inserts. Besides, each of the flutes presents its particular geometry.
(2) Torus end-mills: this due to the fact that we are considering depths of cut within the radius between the primary and secondary cutting edges. This also leads to: a) a varying side cutting-edge angle κ_j; b) varying or linear cutting coefficients.

Following this assumption, the differential force elements associated with the differential edge element (for any of both flutes) can be written as a function of z:

$$\begin{aligned} dF_{t,j}\left(\phi_j,z\right) &= K_{tc,j}f_z\sin\phi_j dz + K_{te,j}ds(z) \\ dF_{r,j}\left(\phi_j,z\right) &= K_{rc,j}f_z\sin\phi_j dz + K_{re,j}ds(z) \\ dF_{a,j}\left(\phi_j,z\right) &= K_{ac,j}f_z\sin\phi_j dz + K_{ae,j}ds(z) \end{aligned} \tag{2}$$

where $K_{tc,j}$-$K_{te,j}$, $K_{rc,j}$-$K_{re,j}$, and $K_{ac,j}$-$K_{ae,j}$ refer, respectively, to the shear-friction pair of coefficients for each direction in the local system of the tool (and for each insert). Projecting these forces on the Cartesian axes, the calculation set leads to the cartesian cutting forces. The effect of side cutting-edge angle can be seen (see also Fig. 3b):

$$\begin{Bmatrix} dF_{x,j}\left(\phi_j,z\right) \\ dF_{y,j}\left(\phi_j,z\right) \\ dF_{z,j}\left(\phi_j,z\right) \end{Bmatrix} = \begin{bmatrix} -\cos\phi_j & -\sin\kappa_j\sin\phi_j & -\cos\kappa_j\sin\phi_j \\ \sin\phi_j & -\sin\kappa_j\cos\phi_j & -\cos\kappa_j\cos\phi_j \\ 0 & \cos\kappa_j & -\sin\kappa_j \end{bmatrix} \begin{Bmatrix} dF_{t,j}\left(\phi_j,z\right) \\ dF_{r,j}\left(\phi_j,z\right) \\ dF_{a,j}\left(\phi_j,z\right) \end{Bmatrix} \tag{3}$$

Finally, the total cutting forces are calculated from the cutting forces acting all over the axial length and considering all the inserts engaged in the cut.

$$F_{xyz}\left(\phi_j\right) = \sum_{j=1}^{Z}\left[\int_{z_1}^{z_2} dF_{xyz,j}\left(\phi_j,z\right)\right] \tag{4}$$

Table 2. Chemical composition of the substrate and coating.

Material	%wt Ti	%wt N	% Al	% C	% W	% Co
Coating	53.36 ± 2.23	24.20 ± 0.85	22.44 ± 1.80	– – -	– – -	– – -
Substrate	– – -	– – -	– – -	12.85 ± 3.90	79.81 ± 3.95	7.35 ± 0.06

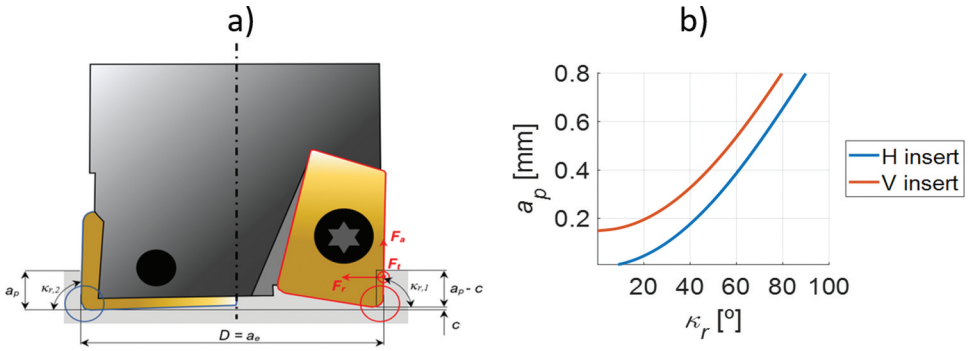

Figure 3. (a) Cutting force trihedron in asymmetric cutter (full immersion, ae = D); (b) Detail of the corner radius.

Figure 3 shows the main cutting parameters and local reference system *tra* for cutting forces, similar at both sides (inserts). The tool also presents an axial offset between both inserts: the starting z is zero for the H-insert while the V–insert begins to cut at 0.15 mm.

For the integration of differential cutting forces, tool local radius $r(z)$ is defined for both tools. Considering the offset c between both inserts:

$$\textit{Insert} \quad H, \qquad r(z) = (0.5D - r_\varepsilon) + \sqrt{r_\varepsilon^2 - (z - r_\varepsilon)^2} \tag{5a}$$

$$\textit{Insert} \quad V, \qquad r(z) = (0.5D - r_\varepsilon) + \sqrt{r_\varepsilon^2 - (z - (r_\varepsilon + c))^2} \tag{5b}$$

Then, the local or instantaneous helix angle (dependent on z) is obtained from:

$$i_j(z) = \tan^{-1}\left(\frac{r(z)}{D/2}\tan\left(\beta_j\right)\right) \tag{6}$$

Finally, the side cutting-edge angle in the corner radius region is variable:

$$\kappa(z) = \sin^{-1}\left(\frac{r(z) - (0.5D - r_\varepsilon)}{0.5D}\right) \tag{7}$$

For coefficients calibration, a set of 23 experiments were done to capture the effect of each of the inserts carefully. Figure 4 presents the experimental acquisition of cutting forces with a Kistler dynamometer. Later, the insert edge is observed to determine the wear progression in both inserts. Table 4 list the

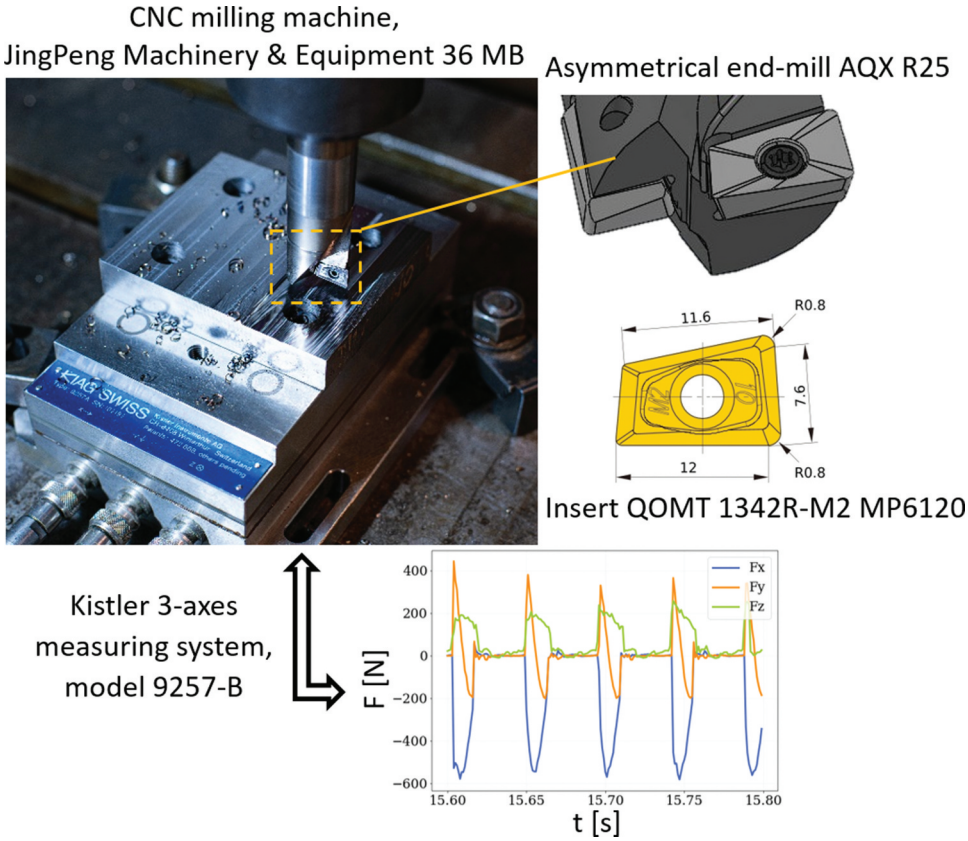

Figure 4. Experimental setup to acquire cutting forces with a Kistler dynamometer.

Table 4. Experimental cutting tests for coefficients calibration.

Test #	Axial depth of cut (mm)	Radial depth of cut (mm)	Feed per tooth [mm/Z/rev]	Feed speed [mm/min]	Insert
1, 11	0.3, 0.8	18	0.10	130	H
2, 12			0.15	195	
3, 13			0.20	260	
4, 14			0.25	325	
5, 15			0.30	390	
6, 16	0.3, 0.8	18	0.10	130	V
7, 17			0.15	195	
8, 18			0.20	260	
9, 19			0.25	325	
10, 20			0.30	390	

configuration of the cutting test to calibrate the cutting coefficients. These cutting tests were performed at two different depths of cut in the corner radius region.

After these cutting tests, the cutting coefficients can be calibrated specifically for each of the tools, see Table 5 and Table 6. It is noted a strong component in the axial direction for low depths of cut where the cutter rubs against the floor. A marked difference between the shear coefficients associated with the H- and V–inserts occurs in tangential and radial components. At low cutting depths, a high component in the tangential direction is noted for both tools and higher friction coefficients suggest intense friction and rubbing mechanisms. The V–insert tends to rub against the workpiece rather than to pure shearing. For higher cutting depths both coefficients tend to behave more similarly to each other. The ratio of the shear coefficients for the tangential component between the H- and V–inserts decreased from 1.67 to 1.22 and for the radial component decreased from 1.74 to 1.18, when the depth of cut increase from 0.3 mm to 0.8 mm. Note also that the friction coefficients are significantly lower than the shear coefficient, even for a higher depth of cut (0.8 mm) smaller friction was observed. The shear coefficient values of the radial versus tangential follow the same trend as in grinding processes, where small depths of cut tend to generate greater radial stresses than tangential stresses.[26]

For validation purposes, the following cutting conditions were proposed with both inserts cutting simultaneously. Only the axial depth of cut and the feed per tooth is modified to

Table 5. Cutting coefficients (c-shear cutting and e-edge/friction) for ap = .3 mm.

Insert	Ktc [MPa]	Kte [N/m]	Krc [MPa]	Kre [N/mm]	Kac [MPa]	Kae [N/m]
H (ap = .3)	1073.1	89.38	1684.6	185.2	1509.2	302.1
V (ap = .3)	640.4	200.9	965.3	213.2	1513.1	459.4
kjH/kjV relation	1.67	0.44	1.74	0.87	0.99	0.66

Table 6. Cutting coefficients (c-shear cutting and e-edge/friction) for ap = 0.8 mm.

Insert	Ktc [MPa]	Kte [N/m]	Krc [MPa]	Kre [N/mm]	Kac [MPa]	Kae [N/m]
H (ap = .8)	895.5	40.3	1891.9	182.3	691.0	140.5
V (ap = .8)	729.2	57.2	1601.8	171.2	740.4	106.7
kjH/kjV relation	1.22	0.70	1.18	1.06	0.93	1.32

Table 7. Validation tests: cutting conditions.

Test #	Axial depth of cut (mm)	Radial depth of cut (mm)	Feed per tooth [mm/Z/rev]	Feed speed [mm/min]	Insert
1	0.3	18	0.20	260	H-V
2	0.8	18	0.25	260	H-V

determine its influence on the cutting forces. Table 7 exhibits the cutting parameters for the model validation. From the validation tests, it can be observed again that the H-insert present higher cutting forces than the V–insert. The model also captures this trend. Specifically, the model tends to overestimate the cutting forces at the V–insert. This is clearly seen for F_z component. A better agreement was satisfied for the high cutting depth. From the three components, the evolution of F_y-F_z is particularly well captured for the tested conditions. Figure 5 shows the modeled and experimental cutting forces in the three components for the two studied cases. The difference between both cases can be illustrated by representing the evolution of chip thickness during one period. Figure 6 shows that due to the axial offset in the V–insert, H-insert is forced to work much more for Case 1. Alternatively, when increasing the depth of cut, both inserts are cutting in a more balanced way.

Wear tests were also performed to track tool wear for the referred cutting conditions of depth of cut of 0.3 and 0.8 mm, see Table 8. Figure 7 shows the wear progression at different machining periods for both inserts until reaching the fracture of the H-insert, in particular about 60 and 95 minutes for depth of cut of 0.8 and 0.3 mm, respectively. Also, tool degradation images are shown after 60 minutes of high feed milling for a depth of cut of 0.8 mm. These V_{Bmax} values were obtained by using scanning electron microscopy. The H-insert presented significant fractures in its cutting edge after that time, but the wear ratio between the two inserts was reduced about 2.9 times, from 9.67 (for a_p = .3 mm) to 3.32 (for a_p = .8 mm). A balanced wear rate was achieved for both inserts by adjusting the depth of cut cutting condition, even though the volume of chips removed increased by 1.68 times (from 359 cm^3 in the initial condition to 604 cm^3 in the proposed one) when the shear capacity limits of the inserts were reached. Therefore, depending on the specific requested cutting conditions, the model clarifies a better margin between both tool progressions.

Conclusions

Asymmetric indexable mills are used because of their high flexibility in milling molds and hard materials, such as P20 steel. These cutting tools lead to productive high-feed conditions in a variety of operations types: contour milling, facing, or slotting with very different ranges of radial and axial cutting depths. This has strong consequences on the inserts' tool life, which can be very different. This aspect is particularly important in the milling of molds where tool wear progression needs to be controlled to save costs and part quality. In this study, a milling force model is proposed for the high feed milling of molds. First, cutting coefficients were obtained from

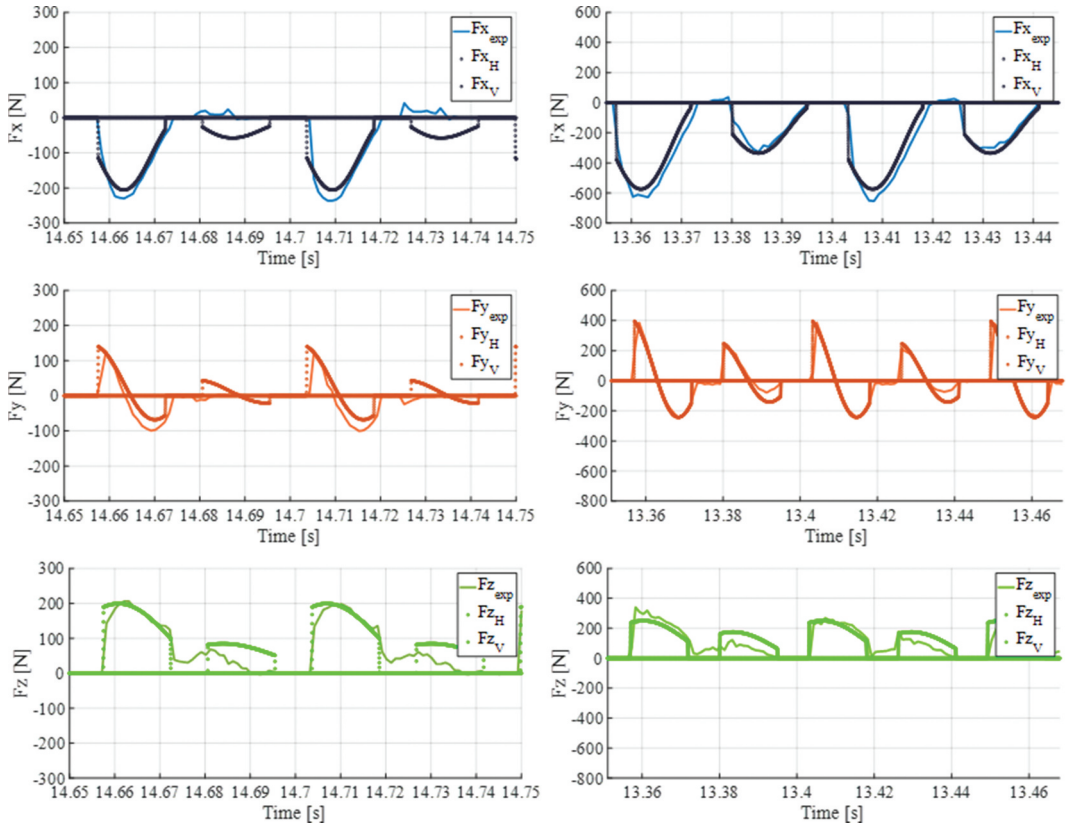

Figure 5. Model validation a. Case 1; b. Case 2.

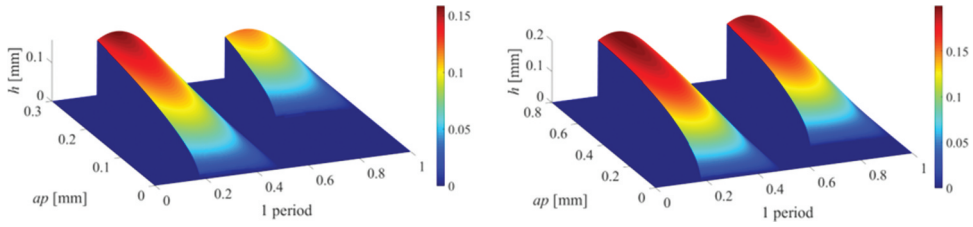

Figure 6. Chip thickness evolution (1 period) a. Case 1; b. Case 2.

Table 8. H- and V–insert wear at *VBmax* for depths of cut of 0.3 and 0.8 mm.

Depth of cut (mm)	Insert Orientation	Time (min)	*VBmax* (µm)	Ratio of VBmáx (H/V)	Chip Removal volumen (cm^3)
0.3	H	95	774	9.67	359.0
	V		80		
0.8	H	60	405	3.32	604.8
	V		122		

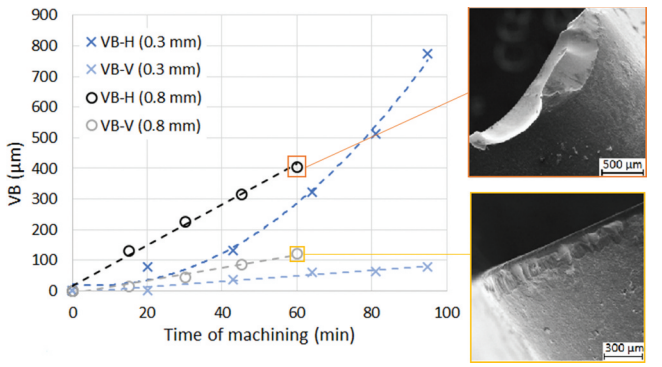

Figure 7. Wear progression for both inserts and tool degradation SEM images after 60 minutes of high feed milling with 0.8 mm of depth of cut.

calibration tests. Then, the model was put to work to find a set of cutting parameters to get a better balance between both tool types. The main contributions are summarized as:

- A new milling force model for axisymmetric bull nose end mills was developed and proposed for a correct balance between cutting inserts. The model captures the behavior of both cutting tools, which were calibrated separately. A good agreement was found between measured cutting forces and modeled ones, specially at high cutting depths.
- The developed model proved its usefulness, as it was possible to balance the wear rate of the H-insert with respect to the V–insert. An increase of 1.7 times in the volume of chips detached was achieved when using a higher depth of cut of 0.8 mm. As predicted by the model, a more favorable set of cutting parameters allows for reduced tool costs and/or improved productivity.
- The cutting forces are related to chip thickness loads on both cutting tools with unbalanced cutting patterns that

can be recognized by comparing the force profiles and peaks on both inserts. Accordingly, the wear ratio between inserts turned from 9.7:1 to 3.3:1 when the depth of cut was increased from 0.3 mm to 0.8 mm, which means unbalance wear reduction of three times.

Nomenclature

a_e	*Radial depth of* cut
a_p	*Depth of cut*
db	*Discrete axial element*
dF	*Cutting forces acting on an infinitesimal edge element*
V_{Bmax}	*Maximum flank wear criterium*
V_c	*Cutting speed*
κ_r	*Cutting edge angle*
K_c	*Shear coefficients*
K_e	*Friction coefficients*
r(z)	*Tool local radius*
tra	*Tool rotating system*
xyz	*Inertial system*

Acknowledgments

We are grateful to Soledad Pereda for helping with Electron Microscopy.

Disclosure statement

All the authors who sign this manuscript do not have any conflict of interest to declare. Furthermore, the corresponding author certifies that this work has not been submitted to or published in any other journal.

Funding

ASE acknowledges the financial support of the Serra Húnter program (Generalitat de Catalunya) reference number UPC-LE-304 (2018). GU also acknowledges the financial support of JANO project with the reference number 2019.0760;Centre for Industrial Technological Development [JANO, 2019.0760];Generalitat de Catalunya [Serra Hunter, UPC-LE-304 (2018)].

ORCID

Gorka Urbicain http://orcid.org/0000-0002-7159-8199
Antonio J. Sánchez Egea http://orcid.org/0000-0001-8085-6869
Daniel Martinez Krahmer http://orcid.org/0000-0002-0184-2168

References

[1] Zanatta, A.; Mesquita, R.; Barbosa, C. Study on the Machinability of VP100 Mold Steel. 20th International Congress of Mechanical Engineering, Gramado, RS, Brazil, 2009.
[2] Roberts, G.; Krauss, G.; Kennedy, R. *Tool Steels*; ASTM International: Ohio, 1998.
[3] Mesquita, R.; Barbosa, C. Desenvolvimento De Aco Com Usinabilidade Melhorada E Acos Endureciveis Por Precipitacao Para Moldes De Plástico. *Tecnol. Metal. Mater. Min.* 2005, *1*(4), 11–15. DOI: 10.4322/tmm.00104003.
[4] Mesquita, R. *Tool Steels, Properties and Performance*; CRC Press: Boca Raton, FL, 2017.
[5] Dewangan, S.; Biswas, C.; Gangopadhyay, S. Influence of Different Tool Electrode Materials on EDMed Surface Integrity of AISI P20 Tool Steel. *Mater. Manuf. Process.* 2014, *29*, 1387–1394. DOI: 10.1080/10426914.2014.930892.
[6] Ji, W.; Liu, X.; Wang, L.; Sun, S. Experimental Evaluation of Polycrystalline Diamond (PCD) Tool Geometries at High Feed Rate in Milling of Titanium Alloy TC11. *Int. J. Adv. Manuf. Technol.* 2014, *77*, 1549–1555. DOI: 10.1007/s00170-014-6517-9.
[7] Metapol, S. A. Aceros Especiales. http://www.metapol.com.ar/ (accessed April 08, 2021).
[8] Zanatta, A.; de Oliveira Gomes, J.; Mesquita, R. Influencia Do Enxofre Na Usinabilidade E Polibilidade De Acos Ferramenta Para Moldes. XII Coloquio de Usinagem, Uberlandia, Brasil, 2008.
[9] Martinez Krahmer, D.; Hameed, S.; Sánchez Egea, A. J.; Pérez, D.; Canales, J.; López de Lacalle, N. Wear and MnS Layer Adhesion in Uncoated Cutting Tools When Dry and Wet Turning Free-Cutting Steels. *Metals*. 2019, *9*, 556. DOI: 10.3390/met9050556.
[10] Martinez Krahmer, D.; Urbikain Pelayo, G.; Sánchez Egea, A. J. Dry Machinability Analyses between Free Cutting, Resulfurized, and Carbon Steels. *Mat. Manuf. Process.* 2020, *35*(4), 1–9. DOI: 10.1080/10426914.2020.1734615.
[11] Priyadarshini, M.; Behera, A.; Biswas, C. Effect of Sub-zero Temperatures on Wear Resistance of AISI P20 Tool Steel. *J. Braz. Soc. Mech. Sci. Eng.* 2020, *42*, 212. DOI: 10.1007/s40430-020-02298-2.
[12] Park, C.; Sim, A.; Ahn, S.; Kang, H.; Chun, E. Influence of Laser Surface Engineering of AISI P20-improved Mold Steel on Wear and Corrosion Behaviors. *Surf. Coat. Tech.* 2019, *377*, 124852. DOI: 10.1016/j.surfcoat.2019.08.006.
[13] Yan, G.; Lu, S.; Zhang, M.; Wang, J.; Yang, X.; Zhang, Z.; Gu, J.; Li, C. Wear and Corrosion Behavior of P20 Steel Surface Modified by Gas Nitriding with Laser Surface Engineering. *Appl. Surf. Sci.* 2020, *530*, 147306. DOI: 10.1016/j.apsusc.2020.147306.
[14] Araujo, A.; Fromentin, G.; Blandenet, P. Investigation on PCD Cutting Edge Geometry for Ti6Al4V High-feed Milling. *Int. J. Adv. Manuf. Technol.* 2020, *111*, 1785–1796. DOI: 10.1007/s00170-020-06086-z.
[15] Zhao, P.; Cheng, K.; Jiang, B.; Zuo, L. Development of the Innovative Differential Tool Wear Modeling for High-feed Milling and Its Experimental Verification. *Proc. Inst. Mech. Eng. B.* 2020, 1–13. DOI: 10.1177/0954405420949226.
[16] Garcia, J.; Collado Cipres, V.; Blomqvist, A.; Kaplan, B. Cemented Carbide Microstructures: A Review. *Int. J. Refract. Met. Hard.* 2019, *80*, 40–68. DOI: 10.1016/j.ijrmhm.2018.12.004.
[17] Zeilmann, R.; Nicola, G.; Vacaro, T.; Teixeira, C.; Heiler, R. Implications of the Reduction of Cutting Fluid in Drilling AISI P20 Steel with Carbide Tools. *Int. J. Adv. Manuf. Technol.* 2011, *58*, 431–441. DOI: 10.1007/s00170-011-3401-8.
[18] Arruda, E.; Cardoso Brandão, L.; Ribeiro Filho, S.; Aparecido de Oliveira, J. Integrated Optimization Using Mixture Design to Confirm the Finishing of AISI P20 Using Different Cutting Strategies and Ball Nose End Mills. *Measurement*. 2014, *47*, 54–63. DOI: 10.1016/j.measurement.2013.08.052.
[19] Urbikain, G.; Alvarez, A.; López de Lacalle, L. N.; Arsuaga, M.; Alonso, M. A.; Veiga, F. A Reliable Turning Process by the Early Use of A Deep Simulation Model at Several Manufacturing Stages. *Machines*. 2017, *5*(2), 1–15. DOI: 10.3390/machines5020015.
[20] Abou-El-Hossein, K.; Kadirgama, K.; Hamdi, M.; Benyounis, K. Prediction of Cutting Force in End-milling Operation of Modified AISI P20 Tool Steel. *J. Mater. Process. Technol.* 2007, *182*, 241–247. DOI: 10.1016/j.jmatprotec.2006.07.037.
[21] Zou, B.; Huang, C.; Liu, Z.; Zhuang, X.; Wang, J. Tool Wear in Ball-End Milling of Cr12MoV Die Steel Using an Indexable Cutter with the Asymmetric Inserts. *Adv. Mat. Res.* 2012, *500*, 111–116. DOI: 10.4028/www.scientific.net/AMR.500.111 .
[22] Płodzień, M.; Żyłka, Ł.; Sułkowicz, P.; Żak, K.; Wojciechowski, S. High-Performance Face Milling of 42CrMo4 Steel: Influence of Entering Angle on the Measured Surface Roughness, Cutting Force and Vibration Amplitude. *Materials*. 2021, *14*, 2196. DOI: 10.3390/ma14092196.
[23] Voestalpine High Performance Metals Argentina S.A, Acero Bohler M238. https://www.acerosboehler.com.ar/es/products/m238/ (accessed April 08, 2021).
[24] López de Lacalle, L. N.; Urbicain, G.; Fernández-Valdivielso, A.; Alvarez, A.; González, H. Wear-dependent Specific Coeficients

in a Mechanistic Model for Turning of Nickel-based Superalloy with Ceramic Tools. *Open Eng.* 2017, *7*(1), 175–184. DOI: 10.1515/eng-2017-0024.

[25] Bhattacharya, A.; Bera, T.; Thakur, A. On Cutter Deflection Profile Errors in End Milling: Modeling and Experimental Validation. *Mater. Manuf. Process.* 2015, 1–9. DOI: 10.1080/10426914.2014.973598.

[26] Wang, G.; Zou, J.; Huang, T.; Pei, H. Grinding Force of 42CrMo Steel in Grind-Hardening. *ICMSE.* 2016, *2016*, 420–426. DOI: 10.2991/icmse-16.2016.70.